A Method for Direct Measurement of Multiaxial Stress-Strain Curves in Sheet Metal

T. FOECKE, M.A. IADICOLA, A. LIN, and S.W. BANOVIC

A method has been developed that allows measurement of stress-strain curves for sheet metal being deformed in multiaxial tension. The strain state is imposed using a modification of the Marciniak in-plane biaxial stretching test. Resulting stresses are measured using a modified X-ray diffraction (XRD) residual stress measurement system. This system is flexible enough to allow spatial mapping of in-plane stress and measurement of stresses at specific locations of interest on the sample, such as developing localizations. Results are presented correlating measurements on a thin strip of AA5182 with data from standard uniaxial tension test. Also presented are experimentally determined curves for this material in balanced biaxial tension in both the rolling and transverse directions.

DOI: 10.1007/s11661-006-9044-y

I. INTRODUCTION

ACCURATE sheet metal forming die designs rely on numerical models, which in turn rely on accurate constitutive laws and experimental data for the material being deformed. Of particular interest to those modeling sheet metal forming processes using the finite element method (FEM) is the shape of the yield locus in stress space, and in particular how the shape, size, and location of the locus changes with strain level. Experimental data in this area would allow modelers to predict and use a forming limit diagram (FLD) formalism in stress space rather than strain space.[1] This would allow the prediction of maximum allowable stresses in a part being formed, which is a potentially more intrinsic property than the maximum strains, which have been shown to be highly path dependent[2] and valid only for linear strain paths (which are seldom seen in production sheet forming[1]).

To map out the yield locus, one must be able to detect yield in a sample that is being loaded along some multiaxial strain path and simultaneously determine the stresses being imposed. The easiest path to measure is uniaxial tension, where the ratio of principal strains ($\rho = \varepsilon_2/\varepsilon_1$) equals –0.5, and the true stress, defined as current load divided by current cross-sectional area, is assumed uniform across the gage section up to the point of localization prior to failure. Measuring the stress-strain behavior along other strain paths is much more difficult and has been attempted in several ways. Tests involving application of simultaneous tension/torsion or internal pressure/torsion on tubular samples have been used to probe the yield locus,[3,4] but this sample geometry is not readily adaptable to flat sheet samples. Other common methods include hydraulic bulge and cruciform sheet testing.

Hydraulic bulge tests are able to produce near balanced biaxial stress states *via* knowledge of the applied pressure,[5] where the stress at the outer surface is calculated using membrane theory. However, this geometry indufces significant out-of-plane bending, which has been shown to affect forming limits[6] and would produce a gradient in the applied stress through the thickness of the sheet. Additionally, in bulge testing, the deformation varies radially, from balanced biaxial tension at the crown to plane strain near the clamped edge. This results in a radial thickness variation. The stress at a point must be calculated based on the local thickness dimension, which is calculated during the test using the measured average strain and assuming a constant volume in the local area of measurement.

Cruciform sheet metal samples have been deformed using orthogonally oriented hydraulic rams,[7] producing various biaxial strain states in the center of the cruciform arms of the sample based upon the imposed elongations. The stress is then determined using the measured strains in the arms as input to a finite element analysis (FEA), or is calculated as force applied to the arms of the sample divided by the arm cross-sectional area (this assumes no interactions between the axes to produce shear stresses within the range of applied loads). Cruciform tests give good accuracy for probing the yield locus at the point of initial yield when the yield detection technique (such as detecting a temperature rise[8]) senses sufficiently small plastic strains. The sample geometry for cruciform samples is an important factor for experimental accuracy and relevance of the data. Some experiments have produced thinned gage sections in the center of samples by carefully machining a thicker plate, while others have added sacrificial additional sheets with holes in the center, forcing

T. FOECKE, Staff Materials Scientist, M.A. IADICOLA and S.W. BANOVIC, Staff Scientists, and A. LIN, Guest Researcher, are with the Metallurgy Division, Department of Commence, National Institute of Standards and Technology, Technology Administration, Gaithersburg, MD 20899, USA. Contact e-mail: tfoecke@nist.gov
Manuscript submitted March 21, 2006.

deformation to occur in the center of the sample. If no thinning or reinforcing plates are used, then the available plastic strain range of most geometries is small (on the order of 4 pct[6]), and can only probe the location of the yield locus, and cannot directly track the evolution of the yield surface with increasing plastic strain. A special geometry has been developed,[8] producing a reduced cross section in the center without thinning, and produces results up to 5 pct plastic strain before localization occurs within the loading sections. All cruciform samples suffer the limitation that some assumptions must be made in order to calculate the applied stress at the center of the sample, either a consititutive law in FEA,[7] assuming the magnitude of shear stresses within the gage section, or an effective cross section over which to divide the applied loads.[7,8]

For an unbiased determination of multiaxial constitutive relations, it is essential that no assumptions about the form of the stress-strain relation be made in advance. Therefore, experimental geometries where the stress state is determined using modeling approaches are to be avoided. To maximize applicability of this test for manufacturing purposes, it is desirable that the sheet not be modified in thickness prior to testing, as removing the layer that has experienced a skin-pass rolling may significantly alter its behavior. A new test has been developed that uses X-ray diffraction (XRD) methods to measure the stress being applied at any point on a multiaxially strained sheet metal sample under load. This method can measure the stresses and strains until localization prior to sample failure.

II. EXPERIMENTAL PROCEDURE

Biaxial deformation states are produced in sheet metal samples using a technique based upon the Raghavan[6] modification of the Marciniak[9] biaxial stretching test. This test has many advantages: the strains are applied in plane to an as-received sheet sample, there is no frictional contact in the region where measurements are to be made, and the initial sample geometry can be varied so as to produce strain states that range from uniaxial tension ($\rho = -0.5$) through plane strain ($\rho = 0$) to balanced biaxial tension ($\rho = 1$) (Figure 1).

As-received 5182-0 aluminum alloy sheet with an initial thickness of 1.0 mm was cut into 15-in.- (381-mm-) square samples. Washers for the test were produced from 1-mm-thick sheets of 1010 mild steel, also cut to 15-in. (381-mm) squares, by drilling and deburring a 3-in.- (76.2-mm-) diameter hole in the center (Figure 2). Each sample was loaded in a manner described previously[10, 11] at 0.5 mm/s between hold points, where the stress was measured with the sample under load.

The macroscopic plastic strains were measured optically as the change in size and shape of an array of lithographically printed circles using the video system described previously.[10] At each macroscopic plastic strain level, the stress is determined by measuring the change in interatomic spacing in the grains due to the applied load, from which the elastic strains and then

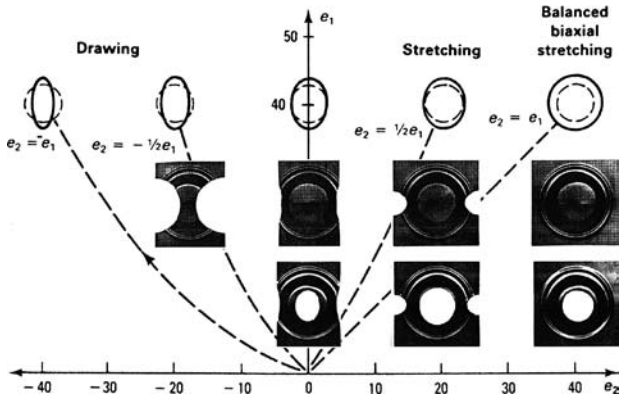

Fig. 1—Strain space description with images of the Rahaven-shaped specimen and matching washers.[6]

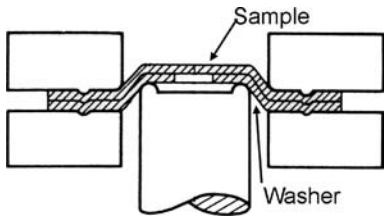

Fig. 2—Through section of Maciniak tooling with the Raghaven specimen and washer.

the stress is calculated. It is important to note that this technique measures two different strains in the sample. The optical technique that tracks the change in the size and shape of a feduciary circle on the surface provides the macroscopic plastic strain, and the X-ray technique described subsequently measures the elastic strain in the grains, which with the elastic constants reveals the applied stress.

The stresses are measured *in situ* during the test using a modified XRD residual stress measuring system. This technique measures the interatomic spacing using a diffraction peak from a given set of atomic planes within the top 40 μm of the thickness, in the case of aluminum. Because the sheet is in plastic yield, the stress through the thickness is uniformly equal to the flow stress at that point, and the surface stress measurement equals the flow stress. The XRD system has been mounted on the back of the forming equipment (Figure 3), allowing the head to reach inside the tooling and probe the center of the sample while under load. The system is equipped with a three-axis translation stage that moves the X-ray head and allows stresses to be measured at specific locations on the sheet.

The stress measurements are performed using the standard $\sin^2\psi$ technique (as described in Reference 12) with the (331) peak and Co K_α radiation for our aluminum samples. We briefly review this technique here for completeness and understanding. As mentioned above, the XRD technique measures the motion of diffraction peaks to determine the interatomic spacing of a given set of adjacent atomic planes near the surface of the specimen in a small volume of the material

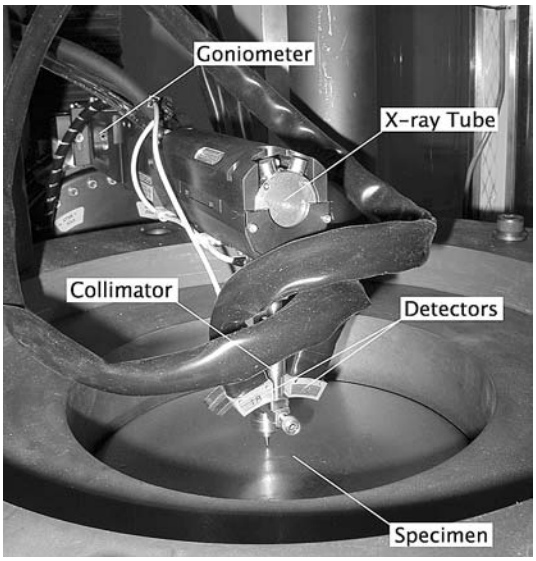

Fig. 3—XRD head in place above the specimen and Marciniak tooling.

(*i.e.*, the focal volume). The governing equation used for residual stress analysis and our *in-situ* stress analysis is

$$\frac{d_\psi - d_o}{d_o} = (\hat{\varepsilon}_{33})_\psi \qquad [1]$$

where the elastic lattice distortion is in terms of the interplanar spacing in the stress-free (d_o) and measured (d_ψ) states and ε_{ij} is the ij component of strain (with the right-hand side in the X-ray source/detector coordinate system). The right-hand side of Eq. [1] may be transformed to the surface coordinate system through a simple rotation (ψ), as shown in Figure 4. Typically, stresses are determined from these average microstrains assuming an isotropic constitutive law:

$$\varepsilon_{ij} = \frac{1+v}{E}\sigma_{ij} + \delta_{ij}\frac{v}{E}\sigma_{kk} \qquad [2]$$

where the terms $-v/E$ and $(1 + v)/E$ are often referred to as the effective or average X-ray elastic constants (XECs) S_1 and $\frac{1}{2}S_2$, respectively. Because the gage area

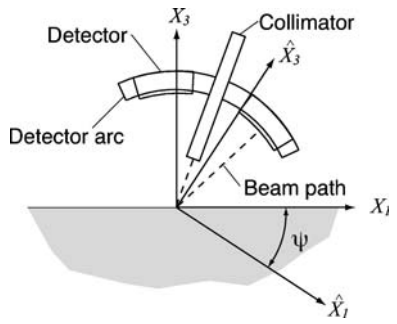

Fig. 4—XRD axes definition.

has stress-free surfaces on top and bottom, and the sheet thickness is quite small as compared to the length and width of the gage section (approximately 3 pct), the assumption is made that $\sigma_{33} = 0$ through the thickness. Therefore our final equation for calculation of stress from the elastic lattice strain is

$$\frac{d_\psi - d_o}{d_\psi} = \frac{1+v}{E}\sigma_{11}\sin^2\psi - \frac{v}{E}(\sigma_{11}+\sigma_{22}) + \frac{1+v}{E}\sigma_{13}\sin 2\psi \qquad [3]$$

The XRD residual stress analysis is performed by plotting elastic lattice distortion *vs* $\sin^2\psi$, where ψ is the current tilt angle at the time of the data collection. Data from multiple tilt angles taken at one stress level are fit with a single line or an ellipse. Note that during sampling, when the angle ψ is set at a specific value, the beam and detector tilt are oscillated during acquisition by a small angle ($\beta = \pm 5$ deg) in addition to the ψ angle to reduce the effect of small surface aberrations on the peak shape. The peaks are located using a Pearson VII fit of the upper 85 pct of the peak with subtraction of the background radiation. From Bragg's law and knowledge of the initial d_o spacing, the lattice distortion is calculated. The slope of the linear fit relates directly to the first term on the right-hand side of Eq. [3], and the intercept relates to the second term. The elliptical fit determines the third term. Although this would suggest that both stresses in the 11 and 22 directions could be determined with one scan, the uncertainties in determination of the second term tend to be too large as compared to the stresses of interest. Therefore, we only measure the stress in the direction of tilt. The shear determined by the elliptical fit (*i.e.*, shear splitting) should not exist in our experimental arrangement because we align the plane of the X-ray head tilt with the principal axes of the deformation in the sheet. Therefore, most (if not all) shear seen is due to misalignments in the system or effects of texture.

Because the system measures the stress in the direction of tilting of the X-ray head, multiple samples that are rotated about the sheet surface normal axis are used to measure the flow curves in many directions within a single strain state. For each stress measurement, the biaxial straining was interrupted and the measurement made within 90 to 180 seconds; then straining was continued. The strain rate used was approximately 1×10^{-4} s^{-1} between measurements.

The XECs used in the measurement are not the single-crystal values, but are effective XECs that must be determined separately to account for crystallographic texture, chemical and alloying effects, and other variables. The $\sin^2\psi$ method can be particularly difficult in samples that exhibit an elevated degree of crystallographic texture,[13] as is typically present in rolled sheet samples. The effective XECs[14] were measured by straining a tapered uniaxial tensile specimen[15] in a portable tensile stage with a calibrated load cell, while simultaneously measuring the tensile stresses using the X-ray system. Correction factors for the XECs were

calculated assuming the gage section of the specimen is under uniaxial stress, which is measured using the load from the load cell and the elastic strain measured through a clip-on extensometer on the back of the sample. This was done in both the rolling and transverse sheet directions. The effective XECs might be expected to change with accumulated plastic strain, because this will change the texture of the sample.[11,16,17] For uniaxial samples, this correction is easily determined using the method described previously while tracking the plastic strains using an extensometer. To determine the effect of biaxial plastic strain, additional samples prestrained in balanced biaxial tension to different plastic strain levels were subsequently tested in uniaxial tension under the X-ray system in the same manner as the unprestrained samples. This permitted calculation of correction factors as for the as-received and balanced biaxial prestrained materials for rolling and transverse directions that were applied to the subsequent stress measurements.

Accurate measurement of the stresses in the sheet using this X-ray technique requires careful experimental setup and interpretation. Several sources of experimental error have been considered and examined. Alignment is very important (ASTM E915[18]), and in this particular system the collimator to surface distance must be accurate within approximately 200 μm to maintain focus. This is checked before each stress measurement. The mathematical fits of the d_o *vs* $\sin^2\psi$ data are elliptical in functionality, but the application of a balanced biaxial strain to the sheet should not produce any shear stresses, which as described previously is the typical cause of elliptical splitting in the data. As a practical matter, the appearance of elliptical splitting in our data indicates that the system is out of proper setup, usually out of focus. The X-ray system alignment and focus are initially checked by performing a stress measurement on a fine powder sample of the same composition (which is assumed to be stress free). The uncertainty of the stress measurements presented here is based on the first standard deviation of the linear fits of the d_o *vs* $\sin^2\psi$ data. This results in a typical uncertainty for the stress measurements presented here of 8.7 MPa. The typical macroscopic plastic strain uncertainty seen was measured to be 0.5 pct.

III. EXPERIMENTAL RESULTS

Experiments incorporating the X-ray technique described in Section II were performed on both uniaxially and equibiaxially strained AA5182 specimens. First we discuss the results for the uniaxial as-received and 20 pct balanced biaxially prestrained specimens, which are used to calibrate the stress measurement technique. Then, the balanced biaxial data are presented with and without the XEC calibration for comparison. Finally, we discuss some simple models often used to develop biaxial behavior based on uniaxial behavior and compare these results with the biaxial data developed in the present study.

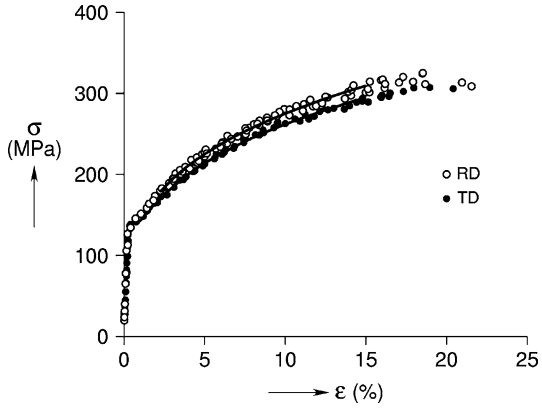

Fig. 5—*In-situ* uniaxial results (circles) with power-law fit curves.

A. *Uniaxial*

As described previously, a small tensile frame with a load cell was built to test ASTM E8 subsized tensile specimens *in situ* (under the X-ray beam) to determine the ability of the X-ray system to measure stresses in highly textured sheet samples undergoing plastic deformation. The true stress (σ)–true strain (ε) results for AA5182 are shown in Figure 5 for the rolling direction (RD, open circles) and transverse direction (TD, closed circles) developed from the load cell and extensometer data. Each data point shown is the result of one XRD stress scan (recall that one scan includes multiple sample angles and takes about 90 to 180 seconds). The data shown are a result of multiple specimens with axial loading oriented in each direction (rolling and transverse). A power law is fit to each data set (over the 2 to 15 pct strain range), and the fits are shown as solid curves in Figure 5 and numerically in Table I. The variability in the stress is not solely a result of the different specimen tested, but is partially due to the serrated yielding seen in AA5182.[19] Figure 6 is a plot of the σ-ε trace for a typical *ex-situ* uniaxial experiment (not under the X-ray system) with a constant strain rate of 1×10^{-3} for a sample oriented transverse to the rolling direction. The stresses measured by the load

Table I. Power-Law ($\sigma = K\varepsilon^n$) Fit Parameters for Various Reported Data (MPa); Values Shown in Braces are Uncertainties Based on One Standard Deviation of the Fit

		Uniaxial (*in-situ*)	Uniaxial (*ex-situ*)	Biaxial (*in-situ*)	Biaxial (*in-situ* with XEC Correction)
0 deg	K	536 [3.53]	565 [3.44]	566 [9.52]	560 [8.35]
	n	0.289 [0.0032]	0.302 [0.0015]	0.256 [0.0064]	0.272 [0.0059]
90 deg	K	514 [2.59]	558 [4.26]	554 [6.85]	460 [9.04]
	n	0.293 [0.0029]	0.316 [0.0016]	0.270 [0.0055]	0.198 [0.0072]

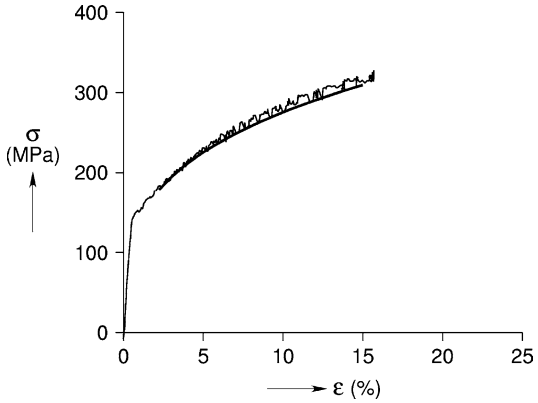

Fig. 6—Serrated yielding seen in uniaxial *ex-situ* results with a power-law fit of the *in-situ* results for specimens oriented transverse to the rolling direction.

cell show clearly the serrated flow of AA5182, indicating a negative strain rate sensitivity. The power-law fit shown in Figure 6 is for the transverse orientation *in-situ* uniaxial data (with multiple hold times, shown in Figure 5). As expected, the data taken at the hold times are recorded after initial relaxation, and thus lie on the lower edge of the serrated flow curve. Note that the values determined for the power-law exponent for both orientations of *in-situ* data are nearly identical (Table I), but that the stress values differ by about 5 pct.

Calibrated XECs are determined by plotting the slope of the linear regression of the $\sin^2\psi$ data (P_1) versus the load cell measured true stress ($\sigma_{11} = P(\Delta L/L)/A_o$). These data, shown in Figure 7, are linearly fit, and the slope of the line equals the average effective XEC $(1 + \nu)/E$. This calibration is needed to accurately measure the stresses *via* XRD.[20] Note that ASTM 1426[20] describes the need for XEC determination. However, the standard procedure subjects the calibration sample to elastic strains only, and uses a strain gage and elastic modulus to measure the current stress for calibration. Therefore, a modification of the standard method is used here so that we can determine how the XECs change with plastic strain level. The linear fit shown in Figure 7 is determined using only the solid points shown, which are along the hardening flow curve (after initial yield to just before the localization prior to failure). Table II lists the values of XEC taken from the literature and the effective constants measured using our system for both orientations (rolling and transverse) and for 0 and 20 pct balanced biaxial prestraining. The differences seen are attributed to the texture and accumulated plastic strain effects on the XECs, which are the subject of an ongoing study.

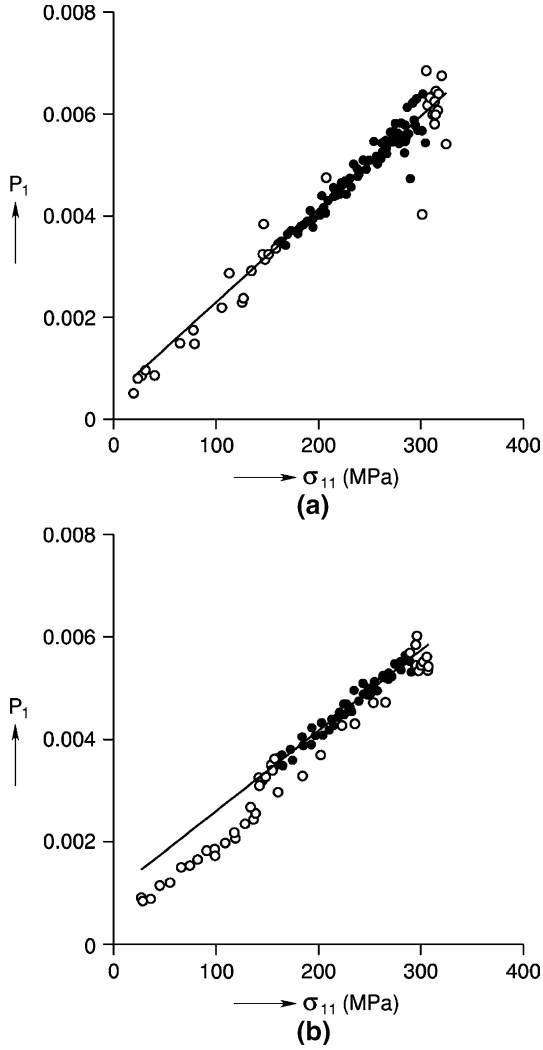

Fig. 7—Comparison of the slope (P_1) of XRD measured lattice strain *vs* $\sin^2\psi$ data and load cell measured stress for the *in-situ* uniaxial experiment in (*a*) the RD and (*b*) the TD. The slope of the linear fits shown here are the calibrated XECs, $(1 + \nu)/E$, for each orientation. Only the solid points are used in the linear regression.

B. *Balanced Biaxial*

A series of tests were performed measuring *in-situ* stresses at various imposed plastic strain levels during balanced biaxial tension using the system default XECs. These results are presented in Figure 8, and may be contrasted to the flow data measured in uniaxial tension Figures 5 and 6. In both the RD and TD, the flow stress at a given biaxial strain level is higher than that measured at the same uniaxial strain level. The coefficients to the power-law strain hardening relation were calculated between 2 and 25 pct plastic strain and are shown in Table I, and the resulting fits are plotted in Figure 8 as a solid curve. The biaxial data was corrected for the effective XECs measured previously (shown in Table II) using linearly interpolated XEC values based on the current plastic strain level. The corrected form of Figure 8 is shown in Figure 9, where the average stress levels are brought closer together but the hardening indexes are seen to diverge (Table I). The yield stress measured in this investigation (using the 0.2 pct strain offset method) was compared to that measured by Banabic[8] using cruciform testing and temperature measurement to probe the initial yield locus, and these values are also shown in Table III. It is seen that there is a good correlation between the balanced biaxial tension yield stresses reported in Reference 8 and the values measured in the rolling and transverse directions in the

Table II. X-Ray Elastic Constants (in GPa^{-1}) from the Literature (for Various Aluminum Alloys) and Determined in the Present Study (for AA5182) Considering Orientation and Balanced Biaxial Prestraining, ε_p;* Taken from Reference 11

	Literature			Calibrated Effective			
	System Default	Al 5083-H33*	Bulk Al*	RD $\varepsilon_p = 0$ Pct	TD $\varepsilon_p = 0$ Pct	RD $\varepsilon_p = 20$ Pct	TD $\varepsilon_p = 20$ Pct
$\frac{(1+\nu)}{E}$	0.01706	0.01817	0.02004	0.018294	0.015709	0.017628	0.018586

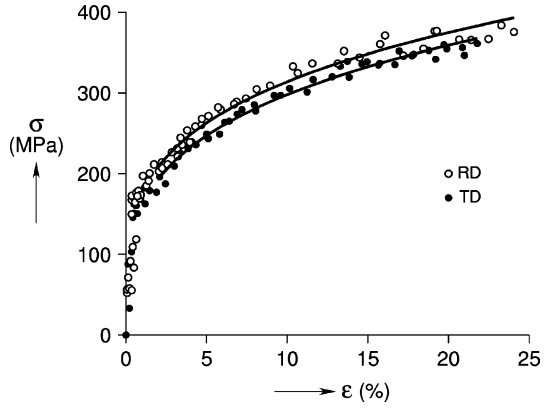

Fig. 8—Biaxial results using default XECs (in the RD and the TD) with power-law fits shown as solid curves.

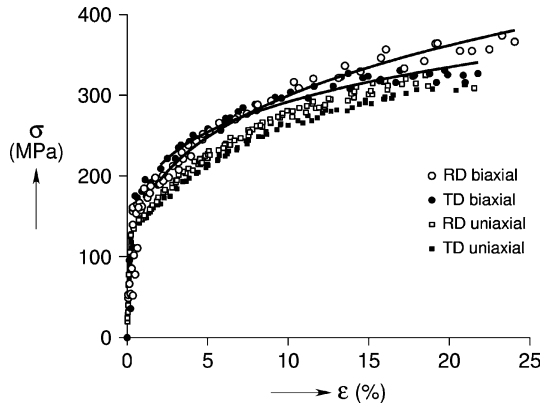

Fig. 9—XEC corrected biaxial results (in the RD, open circles, and the TD, solid circles) with power-law fits shown as solid curves.

present study. Note: the Banabic value assumes isostress conditions.

C. *Discussion*

In simulations of metal forming operations, the uniaxial strain hardening exponent from the power-law hardening relation is often used to predict multiaxial stresses. Multiaxial work hardening can be defined as a change in effective stress with effective strain:

$$n = \frac{d \ln (\sigma^e)}{d \ln (\varepsilon_p^e)} \quad [4]$$

If one uses the von Mises' criterion (assuming plane stress, $\sigma_3 = 0$), the effective stress is given by

$$\sigma^e = \frac{\sqrt{2}}{2}\left[(\sigma_1 - \sigma_2)^2 + (\sigma_2)^2 + (\sigma_1)^2\right]^{\frac{1}{2}} \quad [5]$$

in terms of the principal stresses (σ_1 and σ_2), and the effective plastic strain is given by

$$\varepsilon_p^e = \frac{\sqrt{2}}{3}\left[\left(\varepsilon_1^p - \varepsilon_2^p\right)^2 + \left(\varepsilon_2^p - \varepsilon_3^p\right)^2 + \left(\varepsilon_3^p - \varepsilon_1^p\right)^2\right]^{\frac{1}{2}} \quad [6]$$

in terms of the principal plastic strains (ε_1^p, ε_2^p, and ε_3^p). For a uniaxial tensile test, $\sigma_2 = 0$ and $\varepsilon_2^p = \varepsilon_3^p = -1/2\ \varepsilon_1^p$ (assuming constant volume) . Note: the effective stress-strain curve is the same as the measured uniaxial curve ($\sigma^e = \sigma_1$ and $\varepsilon_p^e = \varepsilon_1^p$) by design. For balanced biaxial tension, $\varepsilon_1^p = \varepsilon_2^p$ and $\sigma_3 = 0$, and assuming constant volume, $\varepsilon_3^p = -2\varepsilon_1^p$. Additionally, the normality requirement results in $\sigma_1 = \sigma_2$. Therefore, the effective values are $\sigma^e = \sigma_1$ and $\varepsilon_p^e = 2\varepsilon_1^p$. Because the effective values are multiples of the uniaxial values, we can define a multiplication factor (f) to convert the uniaxial response to the predicted biaxial response:

$$f_\sigma = \frac{\sigma_1}{(\sigma^e)_{\text{biaxial}}} = 1 \quad \text{and} \quad f_\varepsilon = \frac{\varepsilon_1^p}{(\varepsilon^e)_{\text{biaxial}}} = \frac{1}{2} \quad [7]$$

A similar procedure using the modified Hill criterion[21] would result in biaxial multiplication factors of

$$f_\sigma = \frac{(2+2r)^{1/m}}{2} \quad \text{and} \quad f_\varepsilon = \frac{1}{(2+2r)^{1/m}} \quad [8]$$

Table III. Comparison of Yield Strengths (in MPa) along Various Biaxial Strain Paths from the Present Study (by 0.2 Pct Offset Method) and the Work of Banabic[8] (by Temperature Rise); the First Two Columns Compare Uniaxial Yield Points in the RD and TD, the Second Two Columns the Plane Strain Results, and the Third Pair the Balanced Biaxial Results

	σ_1 (RD)	σ_2 (TD)	PS (RD)	PS (TD)	BB (RD)	BB (TD)
Banabic[8]	143	144	160	157	153	153
Present Study	133 ± 7	137 ± 7	—	—	158 ± 12	163 ± 12

Table IV. Biaxial Equivalent Multiplication Factors of Uniaxial Data Based on Various Models for Model Parameters *m* and *r* Shown

	von Mises'	Hill's $m = 2$ and $r = 0.887$	modified Hill's $m = 1.75$ and $r = 0.887$
f_σ	1	0.971	0.967
f_ε	0.5	0.515	0.468

where r is the plastic strain ratio (measure of the resistance to thinning, refer to ASTM E517[22]) and m is an exponent deduced from experimental data. Banabic[8] reports r-values for their AA5182 specimens, which are used here to determine the weighted average r consistent with ASTM E517, resulting in $r_m = 0.887$. The original Hill criterion had set $m = 2$ for all metals, but Parmar and Mellor[21,23] report m values of 1.7 to 1.8 for soft commercial aluminum. The resulting factors (f) may be found in Table IV. Figure 10 is a plot of the biaxial stress-strain data in the rolling direction (open circles) with solid curves showing the *in-situ* uniaxial power-law fit adjusted by the factors shown in Table IV and the dashed curve is the power-law fit of the biaxial data described in Table I. Using this effective stress and strain construction to develop the biaxial mechanical behavior curves does bring the uniaxial curves closer to the biaxial data, but if one assumes power-law hardening $\sigma = K\varepsilon^n$, the effect of the multiplicative factors ($\sigma_1 = (f_\sigma/f_\varepsilon^n)\ K\varepsilon_1{}^n$) would result in a change in the K parameter only. Therefore, the effective stress-strain construction used with the power-law model is not sufficient to predict the change in the strain hardening exponents seen in the biaxial data and Table I. Similar results may be shown for other common models including the modified power-law model ($\sigma = k(\varepsilon{-}\varepsilon_0)^n$) and the Voce model ($\sigma = S_\infty(1 - Ae^{\varepsilon/\varepsilon_c})$), where the changes seen in the fitting parameters for the biaxial data cannot be achieved through the effective stress-strain constructions described previously. The overall result is an overprediction of the biaxial hardening by all of the models considered. This overprediction is greater at higher plastic strain levels, which are the strains typically seen in forming operations.

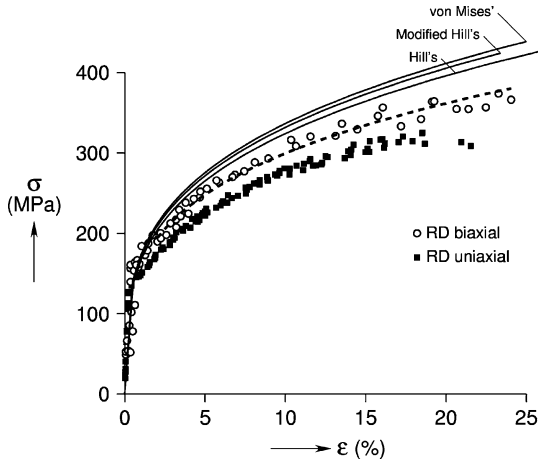

Fig. 10—Comparison of *in-situ* biaxial data in the rolling direction (open circles and dashed curve) and model predictions using the equivalent stress-strain construction and *in-situ* uniaxial power-law fit in the rolling direction.

The results of these analyses are not surprising if one considers the assumptions of the models, which include isotropic material behavior and isostress conditions in balanced biaxial tension. The data in Figure 9 reveal that neither of these results is seen experimentally. The in-plane isostress condition required previously is not met due to crystallographic texture effects, seen by comparing the measured stresses in the rolling and transverse directions in the balanced biaxial test (Figure 9). Additionally, work hardening in balanced biaxial tension is seen to be much lower than that measured in uniaxial tension (Table I). These results are not totally unique, as others have seen that the von Mises' criterion does not fit experimental data,[6] and other laws such as Hill's have been developed to account for crystallographic texture *via* other factors such as the r value.[22] However, none of these studies discuss the possibility of a nonisostress state during balanced biaxial straining. Data generated using the technique developed in the present investigation are being used to study how well current flow models predict the evolution of the yield locus with increasing plastic strain while admitting the possibility of mechanical behavior with texture orientation dependence and nonequal principal stresses during balanced biaxial straining.

IV. CONCLUSIONS

A novel methodology for measuring multiaxial, in-plane stress-strain curves in sheet metal has been presented. The method involved no modification of the sheet beyond trimming to size and shape well outside of the gage section and can be used on iron-, aluminum-, and copper-based alloys. Balanced biaxial stress-strain curves were measured in 5182 aluminum alloy sheet samples, and the results are compared to the strengths and hardening exponents of the same material measured in uniaxial tension in the RD and TD of the sheet. This method is currently being applied to determine how the yield locus varies for a number of different alloys as a function of plastic strain and multiaxial prestrains.

REFERENCES

1. T.B. Stoughton: *J. Eng. Mater. Technol.*, 2001, vol. 123, pp. 417–22.
2. A. Graf and W. Hosford: *Metall. Mater. Trans. A*, 1993, vol. 24A, pp. 2503–12.
3. Z. Chen, S. Maekawa, and T. Takeda: *Metall. Mater. Trans. A*, 1999, vol. 30A, pp. 3069–78.
4. T. Kuwabara, K. Yoshida, K. Narihara, and S. Takahashi: *Int. J. Plasticity*, 2005, vol. 21, pp. 101–17.
5. G. Gutscher, H.-C. Wu, G. Ngaile, and T. Altan: *J. Mater. Processing Technol.*, vol. 146, pp. 1–7.
6. K.S. Raghavan: *Metall. Mater. Trans. A*, 1995, vol. 26A, pp. 2075–20.

7. T. Kuwabara, A. Bael, and E. Iizuka: *Acta Mater*., 2002, vol. 50, pp. 3717–29.
8. D. Banabic: *Annals CIRP*, 2004, vol. 53(1), pp. 219–22.
9. Z. Marciniak and K. Kuczynski: *Int. J. Mech. Sci.*, 1967, vol. 9, pp. 609–20.
10. T. Foecke, S.W. Banovic, and R.J. Fields: *JOM*, 2001, pp. 27–30.
11. S.W. Banovic and T. Foecke: *Metall. Mater. Trans. A*, 2003, vol. 34(3), pp. 657–71.
12. I.C. Noyan and J.B. Cohen: *Residual Stress: Measurement by Diffraction and Interpretation*, Springer-Verlag, New York, NY, 1987.
13. J.A. Pineault, M. Belassel, and M.E. Brauss: *ASM Metals Handbook*, 10th ed., vol.8, *Mechanical Testing*, 2002, ASM, Materials Park, OH, pp. 484–97.
14. K. Perry, I.C. Noyan, P.J. Rudnik, and J.B. Cohen: *Adv. X-ray Analysis*, 1984, vol. 27, pp. 159–70.
15. "Standard Test Method for Uniaxial Tension Test," ASTM E8, ASTM, Philadelphia, PA, 2000.
16. T. Gnaeupel-Herold, T.J. Foecke, H.J. Prask, and R.J. Fields: *Mater. Sci. Eng. A*, 2004, vol. 399(1–2), pp. 26–32.
17. T. Gnaeupel-Herold, H.J. Prask, R.J. Fields, T. Foecke, Z.C. Xia, and U. Lienert: *Mater. Sci. Eng. A*, 2004, vol. 366(1), pp. 104–13.
18. "Standard Test Method for Verifying the Alignment of X-Ray Diffraction Instrumentation for Residual Stress Measurement," ASTM E915, ASTM, Philadelphia, PA, 2002.
19. R.C. Picu, G. Vincze, F. Ozturk, J.J. Gracio, F. Barlat, and A.M. Manniatty: *Mater. Sci. Eng. A*, 2005, vol. 390, pp. 334–43.
20. "Standard Test Method for Determining the Effective Elastic Parameter for X-Ray Diffraction Method of Residual Stress," ASTM E1426, ASTM, Philadelphia, PA, 2003.
21. A. Parmar and P.B. Mellor: *Int. J. Mech. Sci.*, 1978, vol. 20, pp. 385–91.
22. "Standard Test Method for Plastic Strain Ratio r for Sheet Metal," ASTM E517, ASTM, Philadelphia, PA, 2000.
23. A. Parmar and P.B. Mellor: *Int. J. Mech. Sci.*, 1978, vol. 20, pp. 707–20.